

STOCHASTIC VECTOR APPROXIMATE MESSAGE PASSING WITH APPLICATIONS TO PHASE RETRIEVAL

Hajime Ueda, Shun Katakami, Masato Okada[†]

Graduate School of Frontier Sciences, The University of Tokyo, Kashiwa, Chiba 277-8561, Japan

ABSTRACT

Phase retrieval refers to the problem of recovering a high-dimensional vector $\mathbf{x} \in \mathbb{C}^N$ from the magnitude of its linear transform $\mathbf{z} = A\mathbf{x}$, observed through a noisy channel. To improve the ill-posed nature of the inverse problem, it is a common practice to observe the magnitude of linear measurements $\mathbf{z}^{(1)} = A^{(1)}\mathbf{x}, \dots, \mathbf{z}^{(L)} = A^{(L)}\mathbf{x}$ using multiple sensing matrices $A^{(1)}, \dots, A^{(L)}$, with ptychographic imaging being a remarkable example of such strategies. Inspired by existing algorithms for ptychographic reconstruction, we introduce stochasticity to Vector Approximate Message Passing (VAMP), a computationally efficient algorithm applicable to a wide range of Bayesian inverse problems. By testing our approach in the setup of phase retrieval, we show the superior convergence speed of the proposed algorithm.

Index Terms— Phase Retrieval, Bayesian inverse problems, Belief Propagation

1. INTRODUCTION

1.1. Background on Phase Retrieval

Phase retrieval is the problem of recovering a high-dimensional vector $\mathbf{x} \in \mathbb{C}^N$ from the observation $\mathbf{y} \in \mathbb{R}^M$ modeled by

$$\mathbf{z} = A\mathbf{x}, y_\mu \sim p_{\text{out}}(\cdot | |z_\mu|) \quad (\mu = 1, \dots, M) \quad (1)$$

where $A \in \mathbb{C}^{M \times N}$ is the sensing matrix and $p_{\text{out}}(\cdot | |z_\mu|)$ is a probability measure given the magnitude of the μ -th entry of $\mathbf{z} \in \mathbb{C}^M$. A typical application that fits this framework is *Coherent Diffraction Imaging* (CDI) [1], where an object image \mathbf{x} is illuminated by coherent light, and the magnitude of diffracted light is observed in the far field.

It is of practical interest how many observations are needed to recover the signal \mathbf{x} . In recent years, the information-theoretic threshold of sampling ratio has been intensively studied for phase retrieval with large random sensing matrices [2]. From an algorithmic viewpoint, spectral method [3, 4, 5] is known to be an efficient algorithm for obtaining

an estimate $\hat{\mathbf{x}}$ correlated with \mathbf{x} , which is often employed to initialize iterative solvers, including the Wirtinger flow [6], and message passing algorithms [7].

In computational imaging, there are mainly two strategies to improve the ill-posed nature of phase reconstruction – *multiple sensing matrices* and *exploitation of prior knowledge*. A remarkable example of the former is *ptychography* in CDI, where the magnitudes of several linear measurements $\mathbf{z}^{(1)} = A^{(1)}\mathbf{x}, \dots, \mathbf{z}^{(L)} = A^{(L)}\mathbf{x}$ are observed: In a typical setting of ptychography, each sensing matrix $A^{(l)} \in \mathbb{C}^{\bar{M} \times N}$ ($l = 1, \dots, L$) is given as $A^{(l)} = FPS^{(l)}$, where $F \in \mathbb{C}^{\bar{M} \times \bar{M}}$ is the 2D DFT, $P \in \mathbb{C}^{\bar{M} \times \bar{M}}$ is a diagonal matrix, and $S^{(l)} \in \{0, 1\}^{\bar{M} \times N}$ is a binary matrix consisting of \bar{M} row vectors of the identity matrix I_N . On the forward model of ptychography, see, for example, [5, 8]. Another example is *coded diffraction pattern* [9], whose sensing matrices are expressed as $A^{(l)} = FP^{(l)}$, where $F \in \mathbb{C}^{N \times N}$ is the 2D DFT and $P^{(l)} = \text{Diag}(e^{j\theta_1^{(l)}}, \dots, e^{j\theta_N^{(l)}})$ denotes a random phase modulation. This model corresponds to CDI with "random phase masks" placed after the object \mathbf{x} , as illustrated in Fig. 1. Random masks are actively utilized in CDI experiments [10].

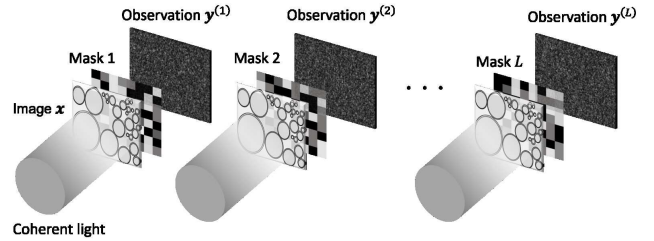


Fig. 1. Setup of coded diffraction pattern

Regarding prior knowledge of the object image, *support constraint* and *sparsity* of \mathbf{x} are frequently exploited in phase retrieval. *Bayesian inference* provides a framework for incorporating such prior knowledge into a statistical model. The Bayes' theorem for the model (1) is written as

$$p(\mathbf{x}, \mathbf{z} | \mathbf{y}) \propto p_{\text{in}}(\mathbf{x}) \delta(\mathbf{z} - A\mathbf{x}) \prod_{\mu=1}^M p_{\text{out}}(y_\mu | |z_\mu|) \quad (2)$$

wherein the prior $p_{\text{in}}(\mathbf{x})$ expresses the prior knowledge on \mathbf{x} ,

[†]H.U. is supported by Advanced AI Talent Development to Lead the Next-Generation Intelligent Society (BOOST NAIS). This work is partly supported by JSPS KAKENHI Grant Number 23H00486, 23K16959, and Digital Transformation Initiative for Green Energy Materials (DX-GEM).

and $\delta(\cdot)$ is the Dirac delta function. To compute the posterior density $p(\mathbf{x}, \mathbf{z}|\mathbf{y})$ in a reasonable computational time, approximation methods such as the mean-field approach and approximate message passing have been successfully applied to phase retrieval. [2, 11, 12]

1.2. Illustration of the key idea

Our approach is to blend the two techniques stated above: multiple measurements and Bayesian inference. We aim to reconstruct a complex image $\mathbf{x} \in \mathbb{C}^N$ from L observations $\mathbf{y}^{(l)} \in \mathbb{R}^M$ ($l = 1, \dots, L$). Using sensing matrices $A^{(1)}, \dots, A^{(L)} \in \mathbb{C}^{M \times N}$, the observations are modeled by

$$\mathbf{z}^{(l)} = A^{(l)}\mathbf{x}, \mathbf{y}^{(l)} \sim p_{\text{out}}(\cdot | |\mathbf{z}^{(l)}|) \quad (l = 1, \dots, L) \quad (3)$$

with $p_{\text{out}}(\mathbf{y} | |\mathbf{z}|) \triangleq \prod_{\mu} p_{\text{out}}(y_{\mu} | |z_{\mu}|)$. By defining the concatenated sensing matrix and observation as

$$A = \begin{pmatrix} A^{(1)} \\ \vdots \\ A^{(L)} \end{pmatrix}, \mathbf{z} = \begin{pmatrix} \mathbf{z}^{(1)} \\ \vdots \\ \mathbf{z}^{(L)} \end{pmatrix}, \mathbf{y} = \begin{pmatrix} \mathbf{y}^{(1)} \\ \vdots \\ \mathbf{y}^{(L)} \end{pmatrix} \quad (4)$$

the model (3) is reduced to model (1). However, crucial to our algorithm is sequential access to the observations $\mathbf{y}^{(1)}, \dots, \mathbf{y}^{(L)}$ which leads to faster convergence, compared to accessing all of the observations at once. Indeed, sequential ptychographic solvers such as ePIE [13] is known to effectively avoid bad local minima, as detailed in [14].

To incorporate multiple measurements into a Bayesian framework, we extend Vector Approximate Message Passing (VAMP) [15, 16], an efficient inference algorithm for generalized linear models. Our extension, coined Stochastic VAMP, introduces sequential access to data subsets, significantly speeding up convergence. This method is analogous to Stochastic Gradient Descent in non-convex optimization, where gradients are computed from data subsets, hence the name Stochastic VAMP.

2. STOCHASTIC VAMP

2.1. Derivation of VAMP

We review the derivation of VAMP based on expectation propagation (EP) [15, 16]. For the Bayesian problem in Eq. (1), we start with an equivalent model:

$$p(\mathbf{x}_1, \mathbf{x}_2, \mathbf{z}_1, \mathbf{z}_2|\mathbf{y}) \propto p_{\text{in}}(\mathbf{x}_1)\delta(\mathbf{x}_1 - \mathbf{x}_2) \times \delta(A\mathbf{x}_2 - \mathbf{z}_2)\delta(\mathbf{z}_1 - \mathbf{z}_2)p_{\text{out}}(\mathbf{y}||\mathbf{z}_1|) \quad (5)$$

The corresponding factor graph is shown in Fig.2 (a). In belief propagation (BP) [17], probability distributions called *messages* are passed through the graph to form *beliefs*, which are the estimates of marginal distributions of each variable. EP approximates messages by using Gaussian. Applying EP to the graph in Fig.2 (a) yields the VAMP algorithm.

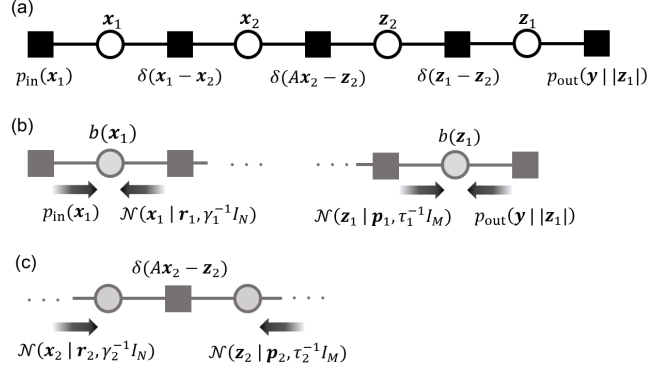


Fig. 2. (a) Factor graph (b) Denoising (c) LMMSE estimation

Here, we outline the update rules of VAMP. Each iteration includes two steps: *denoising* and *LMMSE estimation*. In the denoising part, x_1 node inputs the message $\mathcal{N}(x_1 | \mathbf{r}_1, \gamma_1^{-1} I_N)$ from $\delta(x_1 - x_2)$ node.¹ This creates the belief $b(x_1) \propto p_{\text{in}}(x_1)\mathcal{N}(x_1 | \mathbf{r}_1, \gamma_1^{-1} I_N)$. Denoting expectation w.r.t. measure $b(x_1)$ by $\mathbb{E}[\cdot | b(x_1)]$, the denoiser functions are defined as

$$\mathbf{g}_x(\mathbf{r}_1, \gamma_1) = \mathbb{E}[x_1 | b(x_1)] \quad (6)$$

$$\mathbf{g}'_x(\mathbf{r}_1, \gamma_1) = \frac{1}{N} \mathbb{E}[\|x_1 - \mathbf{g}_x(\mathbf{r}_1, \gamma_1)\|_2^2 | b(x_1)] \quad (7)$$

$b(x_1)$ is approximated by $\mathcal{N}(x_1 | \hat{x}_1, \eta_1^{-1} I_N)$ with

$$\mathbf{x}_1 = \mathbf{g}_x(\mathbf{r}_1, \gamma_1), \eta_1^{-1} = \mathbf{g}'_x(\mathbf{r}_1, \gamma_1) \quad (8)$$

Then, the message $\mathcal{N}(x_2 | \mathbf{r}_2, \gamma_2^{-1} I_N)$ is sent to x_2 node from $\delta(x_1 - x_2)$ node, which, by the rules of BP, is given by

$$\gamma_2 = \eta_1 - \gamma_1, \mathbf{r}_2 = (\eta_1 \hat{x}_1 - \gamma_1 \mathbf{r}_1) / \gamma_2 \quad (9)$$

Likewise, the message $\mathcal{N}(z_1 | \mathbf{p}, \tau_1^{-1} I_M)$ is input to z_1 node. $\hat{z}_1, \lambda_1, \mathbf{p}_2$, and τ_2 are give by

$$\mathbf{g}_z(\mathbf{p}_1, \tau_1) = \mathbb{E}[z_1 | b(z_1)] \quad (10)$$

$$\mathbf{g}'_z(\mathbf{p}_1, \tau_1) = \frac{1}{M} \mathbb{E}[\|z_1 - \mathbf{g}_z(\mathbf{p}_1, \tau_1)\|_2^2 | b(z_1)] \quad (11)$$

$$\mathbf{z}_1 = \mathbf{g}_z(\mathbf{p}_1, \tau_1), \lambda_1^{-1} = \mathbf{g}'_z(\mathbf{p}_1, \tau_1) \quad (12)$$

$$\tau_2 = \lambda_1 - \tau_1, \mathbf{p}_2 = (\lambda_1 \hat{z}_1 - \tau_1 \mathbf{p}_1) / \tau_2 \quad (13)$$

with $b(z_1) \propto \mathcal{N}(z_1 | \mathbf{p}, \tau_1^{-1} I_M) p_{\text{out}}(\mathbf{y} | |\mathbf{z}_1|)$.

In the LMMSE estimation, joint belief on x_2 and z_2 is given as $b(x_2, z_2) \propto \mathcal{N}(x_2 | \mathbf{r}_2, \gamma_2^{-1} I_N) \times \delta(Ax_2 - z_2) \mathcal{N}(z_2 | \mathbf{p}_2, \tau_2^{-1} I_M)$. Marginalizing $b(x_2, z_2)$ w.r.t. z_2 , we have $b(x_2) \propto \mathcal{N}(x_2 | \mathbf{r}_2, \gamma_2^{-1} I_N) \times \mathcal{N}(Ax_2 | \mathbf{p}_2, \tau_2^{-1} I_M)$. This is then approximated by $\mathcal{N}(x_2 | \hat{x}_2, \eta_2^{-1} I_N)$ with

$$\hat{x}_2 = Q(\gamma_2 \mathbf{r}_2 + \tau_2 A^H \mathbf{p}_2), \eta_2^{-1} = \frac{1}{N} \text{Tr}(Q) \quad (14)$$

$$Q = (\gamma_2 I_N + \tau_2 A^H A)^{-1} \quad (15)$$

¹The density of the complex circular Gaussian distribution is given as $\mathcal{N}(x | \mathbf{r}, \gamma^{-1} I_N) \propto \exp(-\gamma \|x - \mathbf{r}\|_2^2)$, wherein $x, \mathbf{r} \in \mathbb{C}^N$ and $\gamma > 0$.

In the rest of this paper, we focus on the case where $A^H A$ is diagonal, thus the matrix inversion in Eq. (15) is not the dominant computational cost. For general sensing matrices, per-iteration matrix inversion can be avoided by pre-computing the singular value decomposition of A . Similarly, $b(z_2)$ is approximated by $\mathcal{N}(z_2|\hat{z}_2, \lambda_2^{-1}I_M)$ with

$$\hat{z}_2 = A\hat{x}_2, \lambda_2^{-1} = \frac{1}{M}\text{Tr}(AQ A^H) \quad (16)$$

The messages $\mathcal{N}(x_1|\mathbf{r}_1, \gamma_1^{-1}I_N)$ and $\mathcal{N}(z_1|\mathbf{p}, \tau_1^{-1}I_M)$ are updated according to

$$\gamma_1 = \eta_2 - \gamma_2, \mathbf{r}_1 = (\eta_2\hat{x}_2 - \gamma_2\mathbf{r}_2)/\gamma_1 \quad (17)$$

$$\tau_1 = \lambda_2 - \tau_2, \mathbf{p}_1 = (\lambda_2\hat{z}_2 - \tau_2\mathbf{p}_2)/\tau_1 \quad (18)$$

which closes the VAMP iteration.

2.2. Stochastic VAMP

A natural extension of VAMP to multiple measurements is derived by EP on the factor graph in Fig.3. Denote the message sent from $\delta(z_1^{(l)} - z_2^{(l)})$ to $z_1^{(l)}$ and the message sent from $\delta(z_1^{(l)} - z_2^{(l)})$ to $z_2^{(l)}$ by $\mathcal{N}(z_1^{(l)}|\mathbf{p}_1^{(l)}, (\tau_1^{(l)})^{-1}I_M)$ and $\mathcal{N}(z_2^{(l)}|\mathbf{p}_2^{(l)}, (\tau_2^{(l)})^{-1}I_M)$, respectively. It is straight forward to derive the LMMSE estimator to update $(\mathbf{p}_1^{(l)}, \tau_1^{(l)})$ and $(\mathbf{p}_2^{(l)}, \tau_2^{(l)})$ for $l = 1, \dots, L$. Note that if we update these L messages in parallel, the resulting algorithm is essentially the same as VAMP with the sensing matrix A and observation \mathbf{y} defined in Eq. (4). The only difference from VAMP is that we allow $\{\tau_1^{(l)}, \tau_2^{(l)}\}$ ($l = 1, \dots, L$) to take different values. However, we can also update L messages sequentially, yielding Stochastic VAMP specified in Algorithm 1.

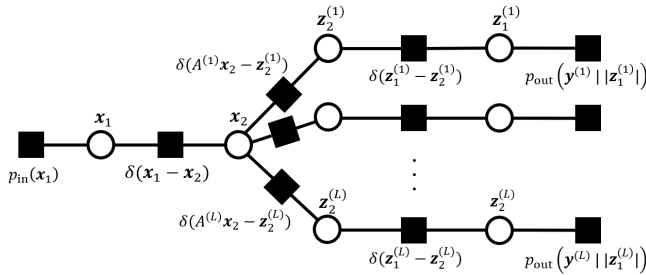


Fig. 3. Factor graph of stochastic VAMP

2.3. Algorithmic detail

We note some implementation details of Stochastic VAMP. Typically, damping is used in the denoising step to help VAMP converge, with the update rule $\hat{x}_{1k} = \rho \mathbf{g}_x(\mathbf{r}_{1k}, \gamma_{1k}) + (1 - \rho)\hat{x}_{1(k-1)}$ and so on, where $0 < \rho < 1$. For unstructured matrix such as Haar distributed A in Sec.3.2, Stochastic

VAMP does not need damping. For the sensing matrices of coded diffraction pattern, a small amount of damping is helpful. In Sec.3.3, we used damping parameter $\rho = 0.95$.

Secondly, when each matrix $A^{(l)}$ have $(A^{(l)})^H A^{(l)}$ diagonal, the matrix inversion in line 5 adds only minor complexity to the algorithm. The dominant computational cost comes from the matrix-vector multiplications in lines 6 and 7. In the case of coded diffraction patterns, the main computational cost is $2L$ FFTs per iteration. For general sensing matrices with non-diagonal $A^H A$, costly matrix-inversion can still be avoided by using the graphical model introduced for D-VAMP [18] and pre-computing the singular value decompositions of $A^{(1)}, \dots, A^{(L)}$.

Lastly, in our experiments, we assumed that the SNR and prior are known, but they can be learned from the dataset using methods from [19]. Although noise learning and multiple restarts can help phase retrieval algorithms avoid bad local minima [11, 12], numerical results indicate that Stochastic VAMP remains stable even without these enhancements.

Algorithm 1 Stochastic VAMP

Require: Sensing matrices $A^{(1)}, \dots, A^{(L)}$, observations $\mathbf{y}^{(1)}, \dots, \mathbf{y}^{(L)}$, number of iterations K_{it}

- 1: Initialize $\mathbf{r}_{20}, \gamma_{20} > 0$ and $\mathbf{p}_{20}, \tau_{20} > 0$ ($l = 1, \dots, L$)
 - 2: **for** $k = 0, 1, \dots, K_{it}$ **do**
 - 3: **for** $l = 1, \dots, L$ **do**
 - 4: //LMMSE estimation
 - 5: $Q = (\gamma_{2k}I_N + \sum_{l=1}^L \tau_{2k}^{(l)}(A^{(l)})^H A^{(l)})^{-1}$
 - 6: $\hat{x}_{2k} = Q(\gamma_{2k}\mathbf{r}_{2k} + \sum_{l=1}^L \tau_{2k}^{(l)}(A^{(l)})^H \mathbf{p}_{2k}^{(l)})$
 - 7: $\eta_{2k}^{-1} = \frac{1}{N}\text{Tr}(Q)$
 - 8: $\hat{z}_{2k} = A^{(l)}\hat{x}_{2k}$
 - 9: $(\lambda_{2k}^{(l)})^{-1} = \frac{1}{M}\text{Tr}(A^{(l)}Q(A^{(l)})^H)$
 - 10: // Message passing
 - 11: $\gamma_{1k} = \eta_{2k} - \gamma_{2k}$
 - 12: $\mathbf{r}_{1k} = (\eta_{2k}\hat{x}_{2k} - \gamma_{2k}\mathbf{r}_{2k})/\gamma_{1k}$
 - 13: $\tau_{1k}^{(l)} = \lambda_{2k}^{(l)} - \tau_{2k}^{(l)}$
 - 14: $\mathbf{p}_{1k}^{(l)} = (\lambda_{2k}^{(l)}\hat{z}_{2k} - \tau_{2k}^{(l)}\mathbf{p}_{2k}^{(l)})/\tau_{1k}^{(l)}$
 - 15: //Denoising
 - 16: $\hat{x}_{1k} = \mathbf{g}_x(\mathbf{r}_{1k}, \gamma_{1k})$
 - 17: $\eta_{1k}^{-1} = \mathbf{g}'_x(\mathbf{r}_{1k}, \gamma_{1k})$
 - 18: $\hat{z}_{1k}^{(l)} = \mathbf{g}_z(\mathbf{p}_{1k}^{(l)}, \tau_{1k}^{(l)})$
 - 19: $\lambda_{1k}^{-1} = \mathbf{g}'_z(\mathbf{p}_{1k}^{(l)}, \tau_{1k}^{(l)})$
 - 20: // Message passing
 - 21: $\gamma_{2(k+1)} = \eta_{1k} - \gamma_{1k}$
 - 22: $\mathbf{r}_{2(k+1)} = (\eta_{1k}\hat{x}_{1k} - \gamma_{1k}\mathbf{r}_{1k})/\gamma_{2(k+1)}$
 - 23: $\tau_{2(k+1)}^{(l)} = \lambda_{1k}^{(l)} - \tau_{1k}^{(l)}$
 - 24: $\mathbf{p}_{2(k+1)}^{(l)} = (\lambda_{1k}^{(l)}\hat{z}_{1k}^{(l)} - \tau_{1k}^{(l)}\mathbf{p}_{1k}^{(l)})/\tau_{2(k+1)}^{(l)}$
 - 25: **end for**
 - 26: **end for**
 - 27: **Return** \hat{x}_{1k}
-

3. COMPUTATIONAL RESULTS

3.1. Common setup

In this section, we consider an observation model defined as:

$$\mathbf{y} = |\mathbf{z} + \mathbf{w}| \quad (19)$$

where \mathbf{w} is the additive white Gaussian noise (AWGN) given as $\mathbf{w} \sim \mathcal{N}(\cdot|\mathbf{0}, \gamma_w^{-1}I_M)$, and $|\cdot|$ is the element-wise absolute value. The corresponding likelihood function $p_{\text{out}}(\mathbf{y}|\mathbf{z})$ is referred to as the *Rician distribution*, whose denoising functions are derived in [12].

We assume a Gaussian prior $p_{\text{in}}(\mathbf{x}) = \mathcal{N}(\mathbf{x}|\mathbf{0}, I_N)$, but structured priors such as sparse priors can also be used. The total number of observed values is denoted as $M = LM$, where L is the number of sensing matrices $A^{(1)}, \dots, A^{(L)}$ and $A^{(l)} \in \mathbb{C}^{M \times N}$. The sampling ratio is $\alpha \triangleq \frac{M}{N}$.

3.2. Haar distributed sensing matrix

We consider sensing matrices $A^{(l)}$ with $(A^{(l)})^H A^{(l)} = I_{\bar{M}}$ drawn from Haar distribution. In the case of noiseless phase retrieval, the threshold value of α above which VAMP recovers the true signal \mathbf{x} is investigated via asymptotic analysis [2], in which the threshold value for Haar-distributed A is estimated as $\alpha_{\text{FR, Alg}} \simeq 2.265$.

In our experiment, we used $N = 512$, $\alpha = 2.4$, and $L = 2$, with a noise level of 30 dB. We compared Stochastic VAMP with vanilla VAMP, which uses concatenated sensing matrices and observations as in Eq.(4). While VAMP required damping ($\rho = 0.7$) for convergence, no damping was needed for Stochastic VAMP. The true signal \mathbf{x} was drawn from the prior, and both algorithms were randomly initialized. The complexity of both algorithms is similar, with $O((L - 1)N)$ difference per-iteration. The NMSE $\frac{\|\mathbf{x} - \hat{\mathbf{x}}_{1,k}\|^2}{\|\mathbf{x}\|^2}$ is shown against iteration number k in Fig. 4. We observed that the stochasticity significantly accelerates the convergence of the phase retrieval algorithm.

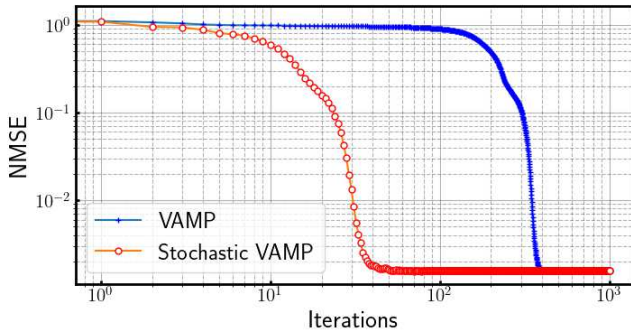


Fig. 4. NMSE versus iteration number for VAMP and Stochastic VAMP.

3.3. Coded diffraction pattern from real world image

In this section, we evaluate the performance of Stochastic VAMP in a more realistic setting. Using the sensing matrix for coded diffraction patterns with $L = 3$ random masks, we conducted numerical experiments on a 256×256 -pixel real-valued image (Fig.5(a)). The SNR is set to 30 dB. A typical reconstruction is shown in Fig.5(b), which was obtained within 20 iterations with a computational time of only **3.9** seconds. Notably, this rapid convergence is impressive, given that conventional phase retrieval algorithms typically require 10^2 to 10^3 iterations for reliable reconstruction. Although we assumed complex Gaussian prior, the reconstruction can be further improved by using non-negative real prior.

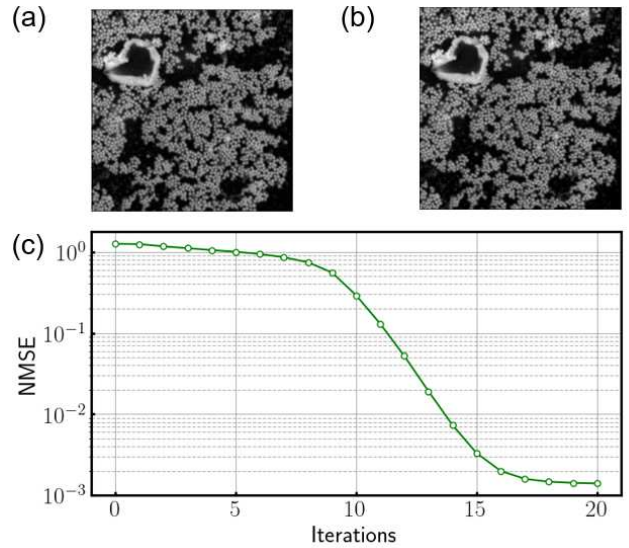


Fig. 5. (a) test image (b) reconstructed image (c) NMSE versus iteration number for Stochastic VAMP.

4. CONCLUSIONS

We enhanced VAMP by introducing stochasticity through non-parallel message updates in belief propagation. In phase retrieval with multiple measurements, our approach significantly accelerates convergence while maintaining the per-iteration complexity of conventional algorithms.

Being a Bayesian approach, our method allows for incorporating prior knowledge, such as image sparsity, similar to [12]. Future work includes applying this approach to ptychographic imaging. Practical ptychographic phase retrieval algorithms such as ePIE perform self-calibration by which both the probe and the object image are reconstructed. Probe reconstruction could be achieved by integrating Stochastic VAMP with techniques from [20, 21].

5. REFERENCES

- [1] Yoav Shechtman, Yonina C. Eldar, Oren Cohen, Henry Nicholas Chapman, Jianwei Miao, and Mordechai Segev, “Phase retrieval with application to optical imaging: A contemporary overview,” *IEEE Signal Processing Magazine*, vol. 32, no. 3, pp. 87–109, 2015.
- [2] Antoine Maillard, Bruno Loureiro, Krzakala Florent, and Lenka Zdeborová, “Phase retrieval in high dimensions: statistical and computational phase transitions,” in *Proceedings of the 34th International Conference on Neural Information Processing Systems*, Red Hook, NY, USA, 2020, NIPS ’20, Curran Associates Inc.
- [3] Marco Mondelli and Andrea Montanari, “Fundamental limits of weak recovery with applications to phase retrieval,” *Foundations of Computational Mathematics*, vol. 19, pp. 703–773, 2017.
- [4] Wangyu Luo, Wael Alghamdi, and Yue M. Lu, “Optimal spectral initialization for signal recovery with applications to phase retrieval,” *IEEE Transactions on Signal Processing*, vol. 67, pp. 2347–2356, 2018.
- [5] Lorenzo Valzania, Jonathan Dong, and Sylvain Gigan, “Accelerating ptychographic reconstructions using spectral initializations,” *Opt. Lett.*, vol. 46, no. 6, pp. 1357–1360, Mar 2021.
- [6] Emmanuel J. Candes, Xiaodong Li, and Mahdi Soltanolkotabi, “Phase retrieval via wirtinger flow: Theory and algorithms,” *IEEE Trans. Inf. Theor.*, vol. 61, no. 4, pp. 1985–2007, apr 2015.
- [7] Marco Mondelli and Ramji Venkataramanan, “Approximate message passing with spectral initialization for generalized linear models,” *Journal of Statistical Mechanics: Theory and Experiment*, vol. 2022, 2020.
- [8] Huibin Chang, Pablo Enfedaque, and Stefano Marchesini, “Blind ptychographic phase retrieval via convergent alternating direction method of multipliers,” *SIAM Journal on Imaging Sciences*, vol. 12, no. 1, pp. 153–185, 2019.
- [9] Emmanuel J. Candès, Xiaodong Li, and Mahdi Soltanolkotabi, “Phase retrieval from coded diffraction patterns,” *Applied and Computational Harmonic Analysis*, vol. 39, no. 2, pp. 277–299, 2015.
- [10] Ryoichi Horisaki, Yusuke Ogura, Masahiko Aino, and Jun Tanida, “Single-shot phase imaging with a coded aperture,” *Opt. Lett.*, vol. 39, no. 22, pp. 6466–6469, Nov 2014.
- [11] Angélique Drémeau and Florent Krzakala, “Phase recovery from a bayesian point of view: The variational approach,” in *2015 IEEE International Conference on Acoustics, Speech and Signal Processing (ICASSP)*, 2015, pp. 3661–3665.
- [12] Philip Schniter and Sundeep Rangan, “Compressive phase retrieval via generalized approximate message passing,” in *2012 50th Annual Allerton Conference on Communication, Control, and Computing (Allerton)*, 2012, pp. 815–822.
- [13] Andrew M. Maiden and John M. Rodenburg, “An improved ptychographical phase retrieval algorithm for diffractive imaging,” *Ultramicroscopy*, vol. 109, no. 10, pp. 1256–1262, 2009.
- [14] Michal Odstrčil, Andreas Menzel, and Manuel Guizar-Sicairos, “Iterative least-squares solver for generalized maximum-likelihood ptychography,” *Opt. Express*, vol. 26, no. 3, pp. 3108–3123, Feb 2018.
- [15] Sundeep Rangan, Philip Schniter, and Alyson K. Fletcher, “Vector approximate message passing,” *IEEE Transactions on Information Theory*, vol. 65, no. 10, pp. 6664–6684, 2019.
- [16] Philip Schniter, Sundeep Rangan, and Alyson K. Fletcher, “Vector approximate message passing for the generalized linear model,” in *2016 50th Asilomar Conference on Signals, Systems and Computers*, 2016, pp. 1525–1529.
- [17] Judea Pearl, *Probabilistic Reasoning in Intelligent Systems: Networks of Plausible Inference*, Morgan Kaufmann Publishers Inc., San Francisco, CA, USA, 1988.
- [18] Mukilan Karuppasamy, Mohamed Akrou, Faouzi Bellili, and Amine Mezghani, “Distributed vector approximate message passing,” in *ICASSP 2024 - 2024 IEEE International Conference on Acoustics, Speech and Signal Processing (ICASSP)*, 2024, pp. 9611–9615.
- [19] Alyson K. Fletcher and Philip Schniter, “Learning and free energies for vector approximate message passing,” in *2017 IEEE International Conference on Acoustics, Speech and Signal Processing (ICASSP)*, 2017, pp. 4247–4251.
- [20] Subrata Sarkar, Alyson K. Fletcher, Sundeep Rangan, and Philip Schniter, “Bilinear recovery using adaptive vector-amp,” *IEEE Transactions on Signal Processing*, vol. 67, no. 13, pp. 3383–3396, 2019.
- [21] Mohamed Akrou, Anis Housseini, Faouzi Bellili, and Amine Mezghani, “Big-vamp: The bilinear generalized vector approximate message algorithm,” in *2022 56th Asilomar Conference on Signals, Systems, and Computers*, 2022, pp. 1377–1384.

↑ TOP of text, page 2 and following pages, aligned to line ↑

↑ TOP of title, centered and aligned to line — page 1 ↑

↑ Author(s) name(s), centered and aligned to line — page 1 ↑

Author affiliation(s), email address(es) centered below names

[Abstract in area between dashed lines — page 1]
[leave two blank lines (12mm) between last line of
Abstract and first line of text.]

Keep all text and graphics within the column margins.

↓ Last line of text must not extend below this line. ↓

[Begin 2nd column of text here — page 1 only]

Keep all text and graphics within the column margins.

↓ Last line of text must not extend below this line. ↓